Cell

Mitochondrial Fusion Protects against Neurodegeneration in the Cerebellum

Hsiuchen Chen,[1] J. Michael McCaffery,[2] and David C. Chan[1,*]
[1] Division of Biology, California Institute of Technology, Pasadena, CA 91125, USA
[2] Integrated Imaging Center, Department of Biology, Johns Hopkins University, Baltimore, MD 21218, USA
*Correspondence: dchan@caltech.edu
DOI 10.1016/j.cell.2007.06.026

SUMMARY

Mutations in the mitochondrial fusion gene *Mfn2* cause the human neurodegenerative disease Charcot-Marie-Tooth type 2A. However, the cellular basis underlying this relationship is poorly understood. By removing *Mfn2* from the cerebellum, we established a model for neurodegeneration caused by loss of mitochondrial fusion. During development and after maturity, Purkinje cells require Mfn2 but not Mfn1 for dendritic outgrowth, spine formation, and cell survival. In vivo, cell culture, and electron microscopy studies indicate that mutant Purkinje cells have aberrant mitochondrial distribution, ultrastructure, and electron transport chain activity. In fibroblasts lacking mitochondrial fusion, the majority of mitochondria lack mitochondrial DNA nucleoids. This deficiency provides a molecular mechanism for the dependence of respiratory activity on mitochondrial fusion. Our results show that exchange of mitochondrial contents is important for mitochondrial function as well as organelle distribution in neurons and have important implications for understanding the mechanisms of neurodegeneration due to perturbations in mitochondrial fusion.

INTRODUCTION

In mammals, three GTPases are required for mitochondrial fusion: Mfn1, Mfn2, and OPA1 (Chen et al., 2005, 2003; Cipolat et al., 2004). Mitochondrial fusion, coupled with the opposing process of fission, controls the morphology of mitochondria and their function, and plays important roles in mammalian development and cell biology. Mice with targeted mutations in *Mfn1*, *Mfn2*, or *OPA1* die embryonically (Alavi et al., 2007; Chen et al., 2003; Davies et al., 2007). Mouse embryonic fibroblasts (MEFs) lacking OPA1 or both Mfn1 and Mfn2 have defects in mitochondrial membrane potential and respiratory capacity (Chen et al., 2005), but the molecular basis of these defects is unknown. In addition, mitochondrial fusion appears to play a protective role in apoptosis (Arnoult et al., 2005; Frezza et al., 2006; Olichon et al., 2003; Sugioka et al., 2004).

Neurons have a particular dependence on precise control of mitochondrial dynamics. Three neurodegenerative diseases are caused by mutations in mitochondrial dynamics genes. Mutations in *Mfn2* cause the autosomal dominant disease Charcot-Marie-Tooth (CMT) type 2A, a peripheral neuropathy of long motor and sensory neurons (Zuchner et al., 2004). Mutations in *OPA1* cause dominant optic atrophy (DOA), the most commonly inherited form of optic nerve degeneration (Alexander et al., 2000; Delettre et al., 2000). Finally, CMT4A is caused by mutations in GDAP1, a protein implicated in mitochondrial fission (Niemann et al., 2005). Other systems underscore the importance of mitochondria in neuronal development and function. Genetic studies in flies suggest that neurons require abundant mitochondria at nerve termini to maintain synaptic transmission and proper ultrastructure (Guo et al., 2005; Stowers et al., 2002; Verstreken et al., 2005). In addition, studies on hippocampal neurons indicate that the growth of dendritic spines is dependent on recruitment of nearby mitochondria (Li et al., 2004).

Although there is clearly an emerging link between defects in mitochondrial fusion and neurodegeneration, its cellular basis is poorly understood. How does loss of mitochondrial fusion affect the mitochondria of neurons, and how do the mitochondria, in turn, affect neuronal function? Why are specific neuronal populations particularly sensitive to changes in mitochondrial dynamics? To address these questions and the general issue of mitochondrial fusion during development, we constructed mice containing conditionally inactivated alleles of *Mfn1* and *Mfn2*. We found that Mfn2, but not Mfn1, is required for proper development and maintenance of the cerebellum. Purkinje cells require Mfn2 for their extensive dendritic outgrowth and survival. Remarkably, fully developed Purkinje cells that subsequently lose Mfn2 also undergo degeneration. These cellular defects are associated with reduced electron transport chain activity, aberrant mitochondrial ultrastructure, and altered mitochondrial distribution.

RESULTS

Mfn1 and *Mfn2* Conditional Alleles

Mfn1 and *Mfn2* knockout ($Mfn1^{null}$ and $Mfn2^{null}$) mice fail to survive past midgestation (Chen et al., 2003). Because this embryonic lethality precludes an examination of the functions of mitochondrial fusion in later development, we constructed conditional knockout alleles for *Mfn1* and *Mfn2* ($Mfn1^{loxP}$ and $Mfn2^{loxP}$; Figure S1 in the Supplemental Data available with this article online). Mating of $Mfn1^{loxP}$ and $Mfn2^{loxP}$ mice to EIIa-Cre mice (Lakso et al., 1996), which express recombinase in all cells, resulted in knockout embryos that die during midgestation, similar to $Mfn1^{null}$ and $Mfn2^{null}$ embryos (data not shown). Moreover, fibroblasts derived from $Mfn1^{loxP}$ and $Mfn2^{loxP}$ animals exhibit Cre-dependent mitochondrial fragmentation (Figure S1).

Roles of Mfn1 and Mfn2 in Placental and Neonatal Development

$Mfn2^{null}$ embryos die in utero due to defects in the trophoblast giant cells of the placenta (Chen et al., 2003). To bypass this problem and examine later development, we used the Meox2-Cre (MORE) line (Tallquist and Soriano, 2000) to target *Mfn2*. Meox2-Cre mice express Cre recombinase throughout the embryo proper by embryonic day 7 but not in cell lineages giving rise to the placenta. Meox2-Cre/$Mfn2^{loxP}$ pups are born at appropriate Mendelian frequencies, confirming that placental insufficiency underlies the embryonic lethality of $Mfn2^{null}$ mice. After birth, however, Meox2-Cre/$Mfn2^{loxP}$ mice exhibit dramatic abnormalities. About one third of Meox2-Cre/$Mfn2^{loxP}$ mice die on postnatal day 1 (P1, where P0 denotes day of birth). Surviving pups show severe defects in movement and balance (Movie S1). They display uncoordinated limb movements, and therefore move primarily by writhing on their abdomens. In addition, they cannot easily regain posture when placed on their backs. They are also severely runted, likely due to feeding problems secondary to their movement disorder. All remaining pups succumb by P17 (Table S1).

To test whether $Mfn1^{null}$ mice also harbor placental defects, we bred the $Mfn1^{loxP}$ mice to Meox2-Cre mice. Remarkably, Meox2-Cre/$Mfn1^{loxP}$ mice survive through adulthood with no obvious defects. Both males and females are fully fertile and healthy to at least one year (Table S1). Therefore, like $Mfn2^{null}$ mice, $Mfn1^{null}$ mice also die due to placental defects. However, because $Mfn1^{null}$ embryos are distinguishable from $Mfn2^{null}$ embryos in appearance and time of death (Chen et al., 2003), Mfn1 and Mfn2 must have essential, nonredundant functions in the placenta.

Despite these nonredundant functions, double-knockout mice ($Mfn1^{null}$, $Mfn2^{null}$) die even earlier than either knockout alone (Chen et al., 2003), indicating that Mfn1 and Mfn2 also have redundant functions during early development. To examine whether this redundant function is also placental, we created an allelic series of Meox2-Cre/Mfn^{loxP} mice (Table S1). Pups of all genotypes are born at expected Mendelian frequencies, but Mfn1-deficient mice lacking one ($Mfn1^{-/-}$, $Mfn2^{+/-}$) or both ($Mfn1^{-/-}$, $Mfn2^{-/-}$) copies of *Mfn2* invariably die on P0. The timing suggests a cardiac, circulatory, or pulmonary cause of death. Mfn2-deficient mice lacking one copy of *Mfn1* ($Mfn1^{+/-}$, $Mfn2^{-/-}$) are indistinguishable from the Mfn2 mutant mice ($Mfn1^{+/+}$, $Mfn2^{-/-}$) described above. As expected, all other pups are normal.

These genetic analyses indicate that Mfn1 and Mfn2 play essential, partially redundant roles in the developing placenta. Furthermore, in contrast to Mfn2, Mfn1 is not required in the mouse proper for normal development. Without Mfn1, however, even the loss of just one allele of *Mfn2* results in perinatal lethality, indicating another critical developmental stage for mitochondrial fusion, and in which Mfn1 and Mfn2 have redundant functions.

Mfn2 Is Required for Postnatal Development of the Cerebellum

To dissect the movement defect of Meox2-Cre/$Mfn2^{loxP}$ mice, we searched for anatomical and histological abnormalities. Beyond changes readily attributable to poor feeding, there is only an obvious reduction in the size of the cerebellum (data not shown). Because the cerebellum controls motor coordination and balance, this abnormality is consistent with the movement defect. To confirm this observation, we turned to two other targeting lines, Wnt1-Cre (Danielian et al., 1998) and En1-Cre (Kimmel et al., 2000). Both lines express Cre recombinase throughout the developing cerebellar primordia, beginning in midgestation, in addition to nonoverlapping domains in other tissues. Wnt1-Cre/$Mfn2^{loxP}$ and En1-Cre/$Mfn2^{loxP}$ mice do indeed recapitulate the movement defect, runting, and early lethality found in Meox2-Cre/$Mfn2^{loxP}$ mice (Figures 1A–1D; Movie S2).

Histological analyses indicate that all three mutant lines have a severe defect in postnatal cerebellar growth (Figures 1F, 2A, and S2). Because expression of the Cre recombinase in the En1-Cre line is most specific for the cerebellar primordia, we present data from the En1-Cre/$Mfn2^{loxP}$ line. Although cerebellar development begins embryonically, a significant portion of development occurs postnatally during the first three weeks (Chizhikov and Millen, 2003; Sotelo, 2004). The mature cerebellum consists of ten lobules, each with three distinct cellular layers (Figure 1E): the outer molecular layer, the densely populated inner granule cell layer, and the intervening monolayer of Purkinje cells (PCs). Between P7 and P16, while the WT cerebellum grows rapidly in size and complexity, the mutant cerebellum instead reduces in size (Figure 1F), suggesting a degenerative process as opposed to lack of development. Using midline sagittal sections, we performed area measurements to quantify this defect. At P5, mutant and WT cerebella have equivalent areas. At P7, however, the areas of mutant cerebella have decreased to approximately 60% of WT. By

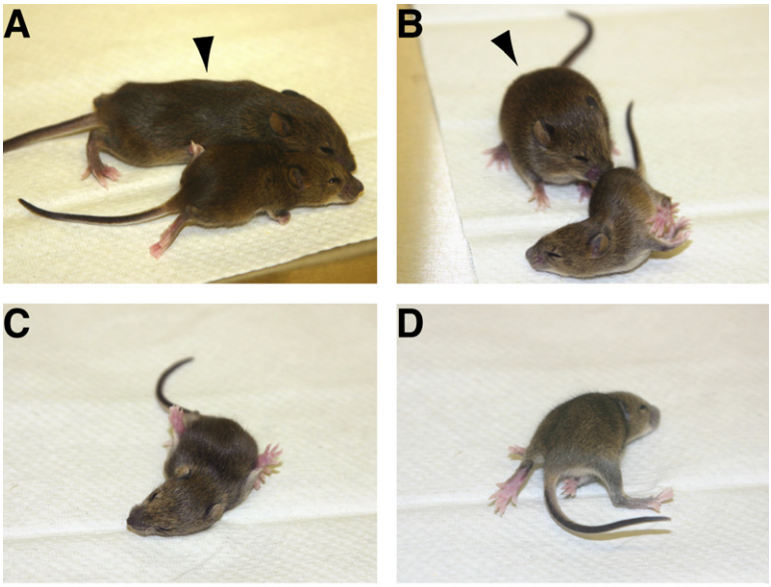

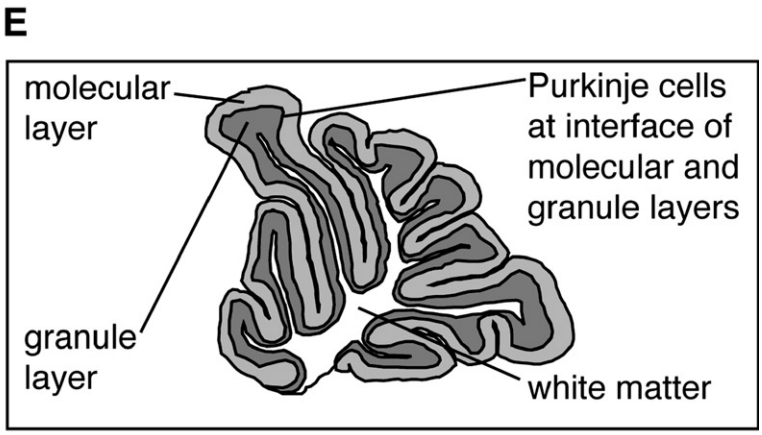

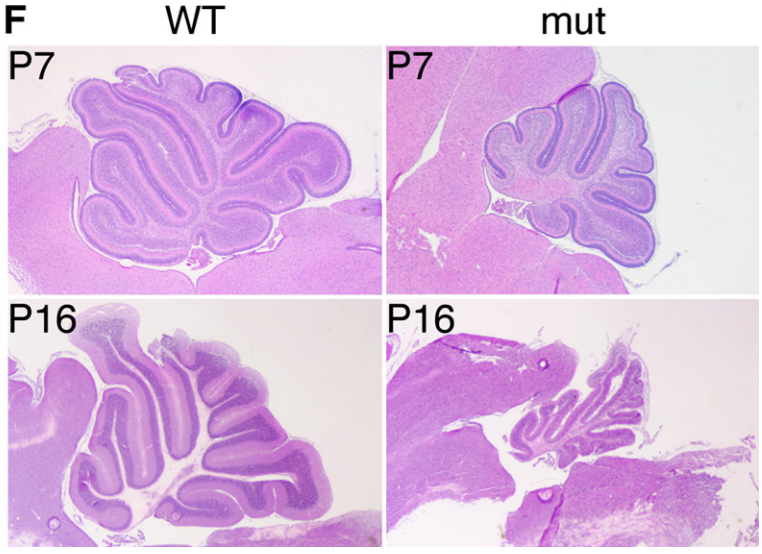

Figure 1. Cerebellar Defect in Mfn2-Deficient Mice

(A–D) Postural and movement defects in Wnt1-Cre/*Mfn2*^{loxP} mice. The WT pup (arrowhead) is larger and remains upright, whereas the runted mutant cannot support itself. Note the contorted posture of the limbs.

(E) Schematic of mature cerebellum. Cellular layers (from surface): molecular layer, Purkinje cells, granule layer, and white matter.

(F) Hematoxylin and eosin stained midsagittal cerebella. In contrast to growth in the WT cerebellum, the En1-Cre/*Mfn2*^{loxP} cerebellum degenerates during this time. Note that P7 cerebella are not fully mature and contain an additional outer layer of external granule cells. These are precursors to fully differentiated granule cells that migrate to the internal granule layer, which is less densely populated here than at P16. 20× magnification.

P15-17, mutant areas drop to about 25% of WT. The molecular layer contributes proportionally the most to this difference in size, because it is only 16% of WT. Despite the clear size reduction, it is important to note that differentiation in terms of lobular organization and formation of the three cellular layers proceeds relatively intact in the mutant cerebellum.

Massive Purkinje Cell Degeneration in Mfn2 Null Cerebella

To determine whether this cerebellar growth defect could be traced to a particular cell layer, we used immunofluorescence (IF) against specific cell markers. Anti-calbindin IF illuminates Purkinje cell bodies and their growing dendrites. PCs are crucial to cerebellar function, because they constitute the sole efferents from the cerebellum, thus relaying all cerebellar output to the rest of the central nervous system. PCs form elaborate dendritic arbors that spread into the molecular layer and synapse with axons of climbing fibers and granule cells. In particular, synapses with the parallel fibers of the granule cells, which contribute to greater than 90% of all PC synaptic connections, provide reciprocal interactions that are important for the survival of both cell types (Sotelo, 2004).

Whereas WT dendritic arbors extend progressively more elaborate processes into the molecular layer during the second postnatal week, the dendrites of En1-Cre/*Mfn2*^{loxP} Purkinje cells show reduced growth and deteriorate over time (Figure 2A). At P10, for example, WT Purkinje cells have dendrites that spread about 50 μm into the molecular layer, but most mutant Purkinje dendrites extend only about 20 μm, are less branched, and have fewer spines (Figure 2B). Because the molecular layer consists largely of PC dendrites, this explains the prominent reduction of the molecular layer described above. During this week, there is a concomitant, widespread loss of Purkinje cell bodies, resulting in very few Purkinje cells by P15 (Figure 2A).

In contrast, we found no difference between mutant and WT migrating granule cells (Figure 2C), indicating that granule cell development proceeds normally. However, markedly higher levels of apoptosis were found in mutant cerebella as early as P6 and continuing through the second postnatal week (Figure 2D). Granule cells clearly undergo apoptosis, likely secondary to insufficient trophic support from PCs. Interestingly, although Mfn2 can protect against apoptosis under some conditions (Sugioka et al., 2004), no TUNEL-positive PCs were seen in mutant cerebella at P5-7, P10, or P15 (data not shown).

Finally, mitochondrial changes are readily apparent early in this process. At P6, F_1F_0-ATPase (Complex V) is expressed at much greater levels in En1Cre/*Mfn2*^{loxP} PCs as compared to controls (Figure 2E). This likely reflects a response to insufficient respiration, as discussed later. Cytochrome *c* (cyt *c*) is similarly expressed more highly (data not shown).

Mitochondrial Fusion Is Required for Proper Mitochondrial Distribution and Outgrowth of Dendritic Spines in Purkinje Cells

To understand the cellular basis of this Purkinje cell defect, we examined Purkinje cells and their mitochondria in mixed cerebellar cultures (Hatten, 1985). Such cultures from neonatal mice recapitulate Purkinje cell differentiation with a time course similar to that in vivo. In these experiments, cerebella were dissected at P1, infected with lentivirus expressing exogenous genes, and cultured as dissociated cells. After two weeks in culture, WT PCs grow elaborate dendritic arbors with many spines, the loci of potential synapses (Figure 3A). Strikingly, En1-Cre/*Mfn2*^{loxP} PCs are largely missing in P14 cultures. In fact, the number of PCs in mutant cultures is only 2% that of WT controls. This cell loss is clearly a degenerative process, because mutant and WT cultures show equal numbers of PCs on P2, and mutant cultures still contain 68% the number of PCs in WT cultures on P7. The few mutant PCs that do survive to P14 exhibit shorter, thinner, less branched dendritic trees with far fewer spines (Figure 3B). Therefore, in vitro cell cultures of dissociated En1-Cre/*Mfn2*^{loxP} cerebella recapitulate the in vivo mouse phenotypes of dendritic attenuation and Purkinje cell death.

Expression of mitochondrially-targeted DsRed shows that mitochondria entirely fill the dendrites of WT Purkinje cells (Figure 3A). Mitochondria in mutant Purkinje cells, however, tend to cluster together in the cell body and do not enter the dendritic tracts (Figure 3B). Because other neuronal systems exhibit a dependence on mitochondrial recruitment for dendritic spine formation (Li et al., 2004), this dearth of dendritic mitochondria probably accounts for the greatly decreased number of spines in Mfn2-deficient PCs. Mutant cells cultured for 7 days also exhibit a similar clustering of mitochondria (Figure 3E), suggesting an inherent distribution defect rather than one secondary to imminent cell death.

Transduction with an Mfn2-expressing lentivirus efficiently rescues the mutant phenotype (Figure 3C). In En1-Cre/*Mfn2*^{loxP} Purkinje cells expressing Mfn2, mitochondria spread throughout the dendrites. Dendritic outgrowth and spine formation are also restored. At P14, Mfn2-expressing mutant cultures contain 46% (up from 2%) the number of PCs in WT cultures. This percentage matches the infection rate, indicating that Mfn2 is highly efficient in Purkinje cell rescue. Therefore, the defect in PCs lacking Mfn2 is likely cell-autonomous, and not dependent on the Mfn2 status of surrounding cells.

Importantly, Mfn1 rescues the mutant phenotype as efficiently as Mfn2. 57% of these PCs survive to P14, again matching the infection rate. These results indicate that the shared ability of these genes to promote mitochondrial fusion is responsible for PC survival, rather than an activity specific to Mfn2. As expected, the fusion-defective mutant, Mfn2^{K109A}, does not rescue the mutant phenotype (data not shown).

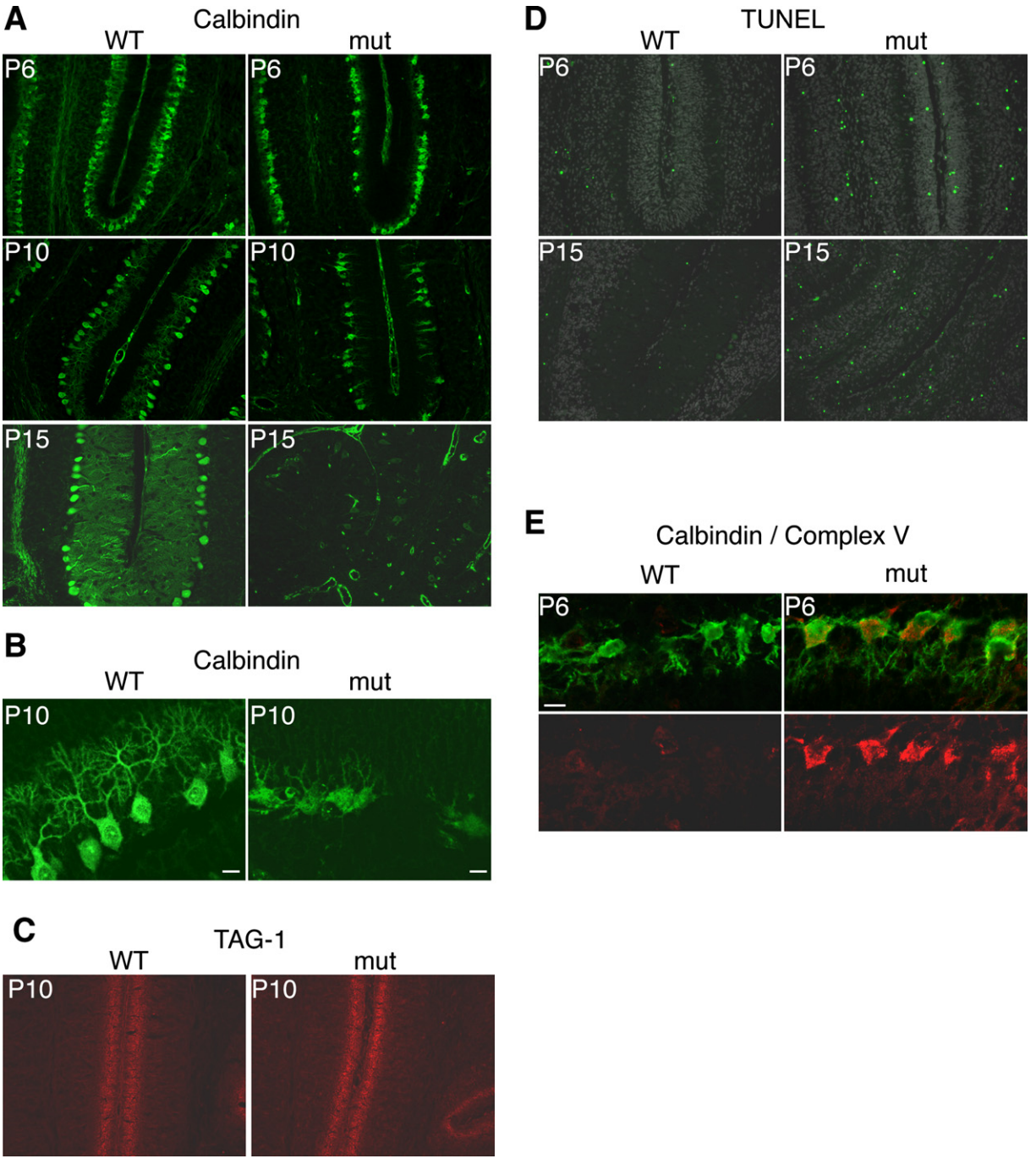

Figure 2. PC Degeneration in En1-Cre/*Mfn2*^{loxP} Cerebellar Sections

(A) Anti-calbindin IF to highlight Purkinje cells. WT PCs display increasingly elaborate dendritic arbors during this time, while mutant PCs show reduced dendritic arbors at P6 and P10 and extensive cell loss at P15.

(B) Confocal images of Purkinje cells at P10. WT Purkinje cells extend dendritic branches deeply into the molecular layer, whereas Mfn2-deficient Purkinje cells have shallow arbors with fewer branches and spines. Scale bars represent 10 μm.

(C) IF for TAG1, a marker of migrating granule cells. No difference is observed between WT and mutant sections.

(D) TUNEL staining (green) for apoptotic cells. Increased apoptosis is apparent throughout the cerebellar layers in the mutant sections. DAPI counterstaining (white) was used to delineate the cellular architecture.

(E) Complex V IF (red) for mitochondria. Mutant PCs (green) show a great increase in Complex V expression. Scale bar represents 10 μm. 200× magnification, except as noted in (B) and (E).

Cell-Autonomous Degeneration of Purkinje Cells

To prove that the defect in Mfn2-deficient PCs is cell-autonomous, we turned to two other Cre excision lines, L7-Cre (Barski et al., 2000) and BACα6-Cre (Aller et al., 2003). L7-Cre expresses solely in the PCs of the cerebellum beginning at P7. Therefore, L7-Cre/*Mfn2*^{loxP} mice address the importance of Mfn2 in mature PCs, as opposed to the developing PCs of En1-Cre/*Mfn2*^{loxP} mice. At first, L7-Cre/*Mfn2*^{loxP} mutants are indistinguishable from WT littermates, but at 2 months of age, they begin to exhibit a slightly shaky gait in the home cage. This unsteadiness increases with time and is exacerbated with tasks requiring more balance, as when walking across a beam (Movie S3). Rotarod analysis was used to quantitate this deficiency in coordination and balance. Whereas WT animals maintain their ability to remain on the rotarod, mutant animals show a progressive decline (Table S2).

Histologically, L7-Cre/*Mfn2*^{loxP} cerebella demonstrate an obvious neurodegeneration over the same time period (Figure 4B). At 1 month of age, mutant PCs are fully developed and indistinguishable from WT PCs. Over the next few weeks, however, degeneration of the dendrites and death of Purkinje cell bodies occur, resulting in very few surviving PCs by 3 months of age. PC axonal changes also occur over this time period. By 7 weeks of age, mutant axons show extensive torpedoes (Figure 4D), focal swellings typical of many neuropathies (Baurle and Grusser-Cornehls, 1994). At 6 months of age, essentially all PCs are gone. DAPI staining demonstrates a collapse of the molecular layer over this time period, while the granule cell layer remains relatively intact (Figure 4C). This suggests that whereas granule cell survival depends on PCs during development, this relationship is less important after cerebellar maturity. TUNEL analysis did not reveal any apoptotic PCs (data not shown).

Midsagittal area measurements show that L7-Cre/*Mfn2*^{loxP} and control cerebella have equal areas at 1 month. However, mitochondrial alterations are already present by this time, as indicated by greatly increased expression of Complex V (Figure 4E) and cyt *c* (data not shown). By 3 months of age, the mutant cerebella are only 75% that of WT. The greatest loss occurs in the molecular layer, with mutants having only 45% the WT area. By 1 year of age, the overall cerebellar area of mutants has dropped to 50% of WT. This primarily reflects further collapse of the molecular layer.

The L7-Cre/*Mfn2*^{loxP} mice definitively show that loss of Mfn2 in PCs causes cell-autonomous neuronal death. In contrast, BACα6-Cre/*Mfn2*^{loxP} mice, which express Cre in mature cerebellar granule cells (Aller et al., 2003), show no defects. BACα6-Cre/*Mfn2*^{loxP} mice still exhibit normal balance at 4 months of age, as tested by rotarod. Histological analysis also revealed no anatomical differences between mutant and control cerebella (data not shown). Therefore, Mfn2 is required in the Purkinje cells of the cerebellum, but not in the far more numerous granule cells, indicating an important cellular distinction in requirements for Mfn2.

Minor Contribution of Mfn1 in Purkinje Cells

Interestingly, an allelic series of *Mfn1* and *Mfn2* mutant PCs indicates that whereas Mfn2 obviously plays a crucial role in PC survival, Mfn1 contributes very little to this process. First, Meox2-Cre/*Mfn1*^{loxP} mice (*Mfn1*$^{-/-}$, *Mfn2*$^{+/+}$), which lack Mfn1 in all cells, demonstrate no movement defect even at 1 year, indicating an intact cerebellum. Furthermore, 9-week-old L7-Cre mice lacking Mfn1 (*Mfn1*$^{-/-}$, *Mfn2*$^{+/-}$) have cerebella containing a uniform, unbroken Purkinje cell monolayer similar to that in WT mice (Figure 5A, calbindin). In contrast, mice lacking Mfn2 (*Mfn1*$^{+/+}$, *Mfn2*$^{-/-}$ or *Mfn1*$^{-/-}$, *Mfn2*$^{-/-}$) demonstrate Purkinje cell death and dendritic attenuation. This comparison indicates that Mfn1 is not required for normal PC survival in the presence of just one WT *Mfn2* allele. It is important to note, however, that there is a minor contribution of Mfn1 to Purkinje survival in the absence of Mfn2. This can be seen in the more severe loss of *Mfn1*$^{-/-}$, *Mfn2*$^{-/-}$ PCs as compared to *Mfn1*$^{+/+}$, *Mfn2*$^{-/-}$ PCs.

Consistent with their contributions to PC survival, RNA in situ analysis of cerebellar sections shows very prominent expression of *Mfn2* (Figure 5C) in PCs but lower expression of *Mfn1* (Figure 5B). In fact, most of the *Mfn1* signal is not located within Purkinje cells, and most likely reflects expression in the candelabrum cells, interneurons that lie between Purkinje cell soma (Laine and Axelrad, 1994). This expression pattern, along with the ability of Mfn1 to rescue cerebellar cultures, suggests that preferential expression of Mfn2 versus Mfn1 in Purkinje cells is the basis for the Mfn2-dependent survival of Purkinje cells.

Dysfunction of the Electron Transport Chain in Purkinje Cells Lacking Mfn2

To determine whether these PC defects are due to problems in mitochondrial function, we analyzed the enzymatic activity of electron transport chain complexes with histochemical stains on fresh frozen sections of cerebella (Figure 5A). 9-week-old L7-Cre/*Mfn2*^{loxP} PCs exhibit a decrease in cytochrome *c* oxidase (COX, Complex IV) activity. In fact, this loss can be seen as early as 6 weeks of age in L7-Cre/*Mfn2*^{loxP} mutants (Figure S3), several weeks prior to the onset of Purkinje cell death. Conversely, there is an increase in succinate dehydrogenase (SDH, Complex II) activity in mutant PCs. COX and SDH stains were performed on adjacent sections to definitively show that low COX activity is not due to the absence of PCs. This combination of low COX and high SDH staining is a hallmark of many myopathies caused by mitochondrial DNA (mtDNA) mutations, and has also been found in muscle fibers during aging (Wallace, 1999). This histochemical profile is believed to indicate loss of electron transport activity with a compensatory increase in mitochondrial biogenesis. The increased expression of Complex V and cyt *c* described above further support this interpretation.

As expected, *Mfn1*$^{-/-}$, *Mfn2*$^{-/-}$ PCs also demonstrate loss of COX activity and higher SDH staining (Figure 5A). However, once again, *Mfn1*$^{-/-}$, *Mfn2*$^{+/-}$ PCs have

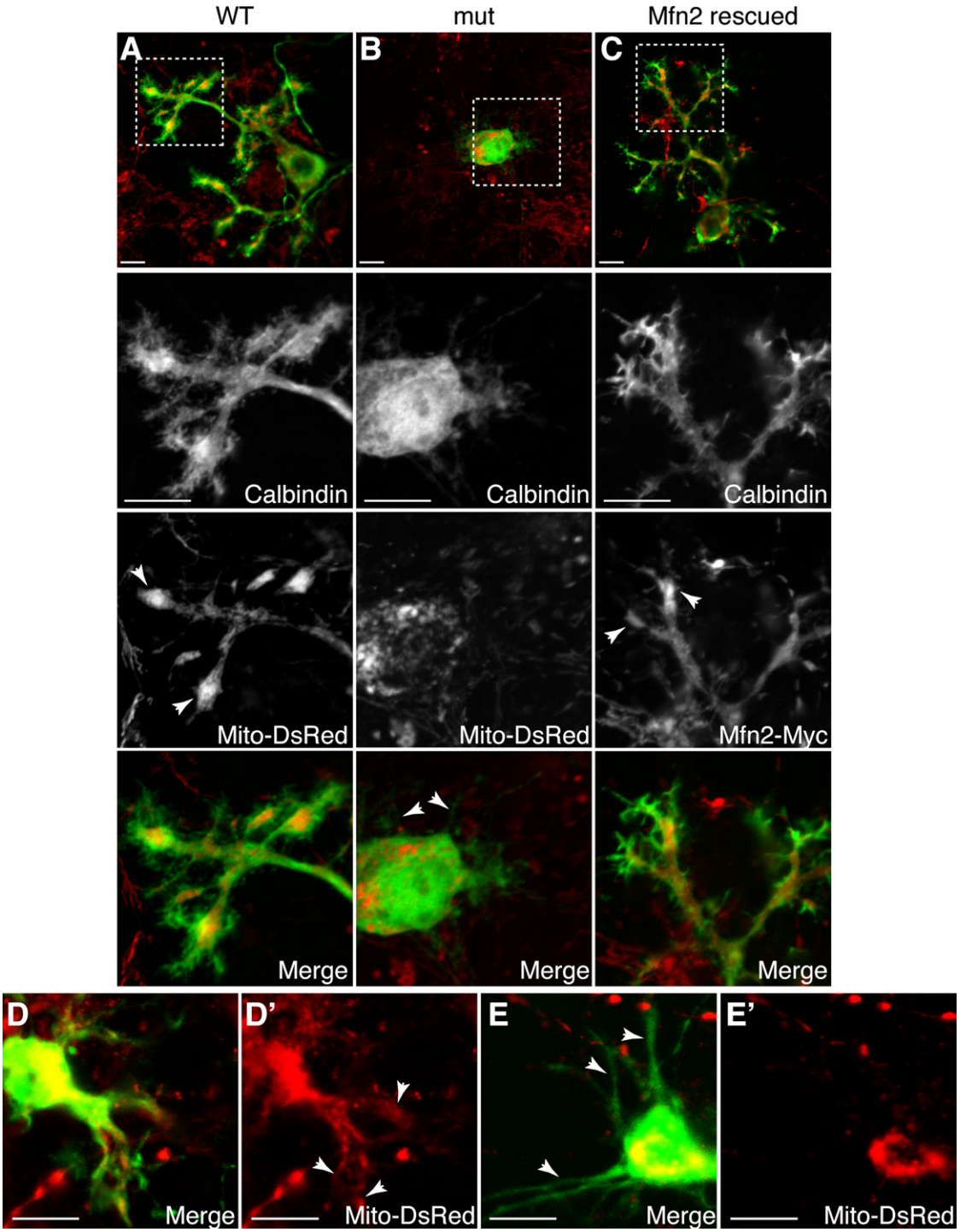

Figure 3. PC Degeneration in En1-Cre/*Mfn2*^{loxP} Cerebellar Cultures

(A) Representative confocal image of PC from a 14 day, WT culture. A low-magnification image showing the Purkinje cell body and dendritic arbor is followed below by high-magnification images of the region boxed. PCs are highlighted with anti-calbindin (green), and mitochondria are labeled with mito-DsRed. Mitochondria of other cells (primarily granule cells) in the culture are also labeled. Note the extensive dendritic branches with feathery spines and densely packed mitochondria throughout (arrowheads).

(B) Mutant PC, with panels as described in (A). In contrast to the WT cells, mutant cells have short and thin dendritic processes (arrowheads) that have few spines. Mitochondria are abundant in the mutant cell body but are sparse in the dendritic branches.

a COX/SDH profile indistinguishable from that of WT PCs, indicating that one WT allele of *Mfn2* provides adequate mitochondrial fusion activity to protect electron transport activity. Staining for NADH dehydrogenase (Complex I) activity demonstrates the same trends as COX for all genotypes (data not shown). Therefore, loss of activity in electron transport chain complexes I and IV precedes neuronal death. Since SDH is the only respiratory complex encoded solely by the nuclear genome, increased Complex II activity suggests that loss of mtDNA may be the causal factor.

Fusion-Deficient Mitochondria Often Lack mtDNA Nucleoids

To examine the relationship between mitochondrial fusion and mtDNA, we stained for mtDNA nucleoids using an anti-DNA antibody. Consistent with previous work (Legros et al., 2004), essentially all WT mitochondria contain at least one mtDNA nucleoid (Figure 6A). *Mfn1*$^{-/-}$ and *Mfn2*$^{-/-}$ MEFs, which have fragmented mitochondria with reduced fusion activity, show loss of mtDNA nucleoids from a significant fraction of mitochondria (Figures 6B and 6C). In Mfn null (*Mfn1*$^{-/-}$, *Mfn2*$^{-/-}$) and OPA1 null cells, which have no fusion activity at all, the majority of mitochondria lack nucleoids (Figures 6D and 6E). Of note, the severity of this heterogeneous mtDNA loss across the different genotypes corresponds well with the severity of mitochondrial membrane potential loss documented previously (Chen et al., 2005; Chen et al., 2003). Technical issues precluded a similar analysis of PCs, but this loss of mtDNA is the likely mechanism for loss of COX and NADH activity.

Ultrastructural Defects in Mfn2 Null PCs

To examine mitochondrial ultrastructure in our mutant PCs, we employed electron microscopy (EM) on P10 En1-Cre/*Mfn2*^{loxP} and 7-week-old L7-Cre/*Mfn2*^{loxP} cerebellar sections (Figure 7). In ultrathin sections from both En1-Cre/*Mfn2*^{loxP} and L7-Cre/*Mfn2*^{loxP} mutants, the Purkinje cells show dramatic defects in mitochondrial morphology, distribution, and cristae organization. The mitochondria are usually larger in diameter and appear round as compared to the elongated, tubular mitochondria found in WT PCs (Figures 7C, 7C′, 7E, and 7E′). Mutant mitochondria also show vesiculation of their inner membranes, in contrast to the regular, accordion-like folds of cristae in WT mitochondria. This combination of large-diameter mitochondria and abnormal cristae structure is often associated with compromised mitochondrial bioenergetics (Bereiter-Hahn and Voth, 1994), and is consistent with the loss of electron transport activity documented by our histochemical stains. The similarity in ultrastructural defects between En1-Cre/*Mfn2*^{loxP} and L7-Cre/*Mfn2*^{loxP} mice is remarkable, and reinforces the conclusion that mitochondrial fusion is required in both developing and mature Purkinje cells.

In addition to these morphological defects, mutant Purkinje cells show aberrant mitochondrial distribution in the dendritic tracks. Whereas mitochondria of WT PCs generally fill the dendritic tracts (Figures 7B and 7D, 7E, and 7F), mitochondria in the dendrites of mutant PCs are far less numerous and those that are present tend to aggregate to the sides (Figures 7B′, 7D′, 7E′, and 7F′). Some images suggest a blockage problem in mutants whereby large, swollen mitochondria cluster at dendritic junctions and are unable to enter the distal, smaller diameter branches (Figure 7F′). Both clustering of mitochondria in the cell body (Figure 7A′) and blockage of dendritic junctions may contribute to the dearth of mitochondria in the dendrites of cultured mutant PCs. It should be noted that in both En1-Cre/*Mfn2*^{loxP} and L7-Cre/*Mfn2*^{loxP} sections, significant variability is seen, with some cells displaying WT structures (Figure 7C′). This is not surprising, because we deliberately chose early ages at which the mutant phenotypes are not yet fully developed to avoid indirect abnormalities secondary to cell death. Interestingly, EM studies on sural nerve biopsies from two CMT2A patients also find clustering of mitochondria and great heterogeneity in structure, with many swollen mitochondria that have irregular membranes (Verhoeven et al., 2006).

Consistent with our in vitro cell culture, in vivo dendritic tracts with abnormal mitochondria have fewer spines (Figures 7D′ and 7E′). In WT Purkinje dendrites at P10, quantitative morphometric analysis of EM sections shows an average spine density of 0.32 spine/μm. In contrast, En1-Cre/*Mfn2*^{loxP} dendrites have a spine density of 0.06 spine/μm. In 7-week-old samples, WT Purkinje dendrites have a spine density of 0.26 spine/μm, compared to 0.05 spine/μm in L7-Cre/*Mfn2*^{loxP} dendrites. Therefore, there is a > 5-fold decrease in the number of spines in mutant dendrites as compared to WT. Since spines are the sites of dendritic synapses, our mutant PCs presumably form far fewer synaptic connections, thus compromising cerebellar function prior to Purkinje cell death.

Finally, as predicted, loss of Mfn1 does not affect mitochondrial morphology (Figure S4), indicating a relatively minor role for Mfn1 in PC mitochondrial fusion. Even when only one WT allele of *Mfn2* is present, mitochondria in Mfn1-deficient PCs are elongated and well distributed in dendritic tracts. Cristae structure is well-preserved, consistent with the normal histochemical profile.

(C) Mfn2-Myc-infected mutant PC, with panels as described in (A), except mitochondria are labeled with anti-Myc staining. Rescued mutant cells have extensive dendritic processes that are filled with mitochondria (arrowheads) and extend numerous spines.
(D) Anti-calbindin (green) IF on WT PC from 7 day culture with mito-DsRed. Arrowheads indicate presence of mitochondria in dendritic extensions.
(E) Mutant PC from 7 day culture, stained as in (D). As on P14, mitochondria are congregated in the cell body and are missing from the thin dendritic extensions (arrowheads).
Scale bars indicate 10 μm.

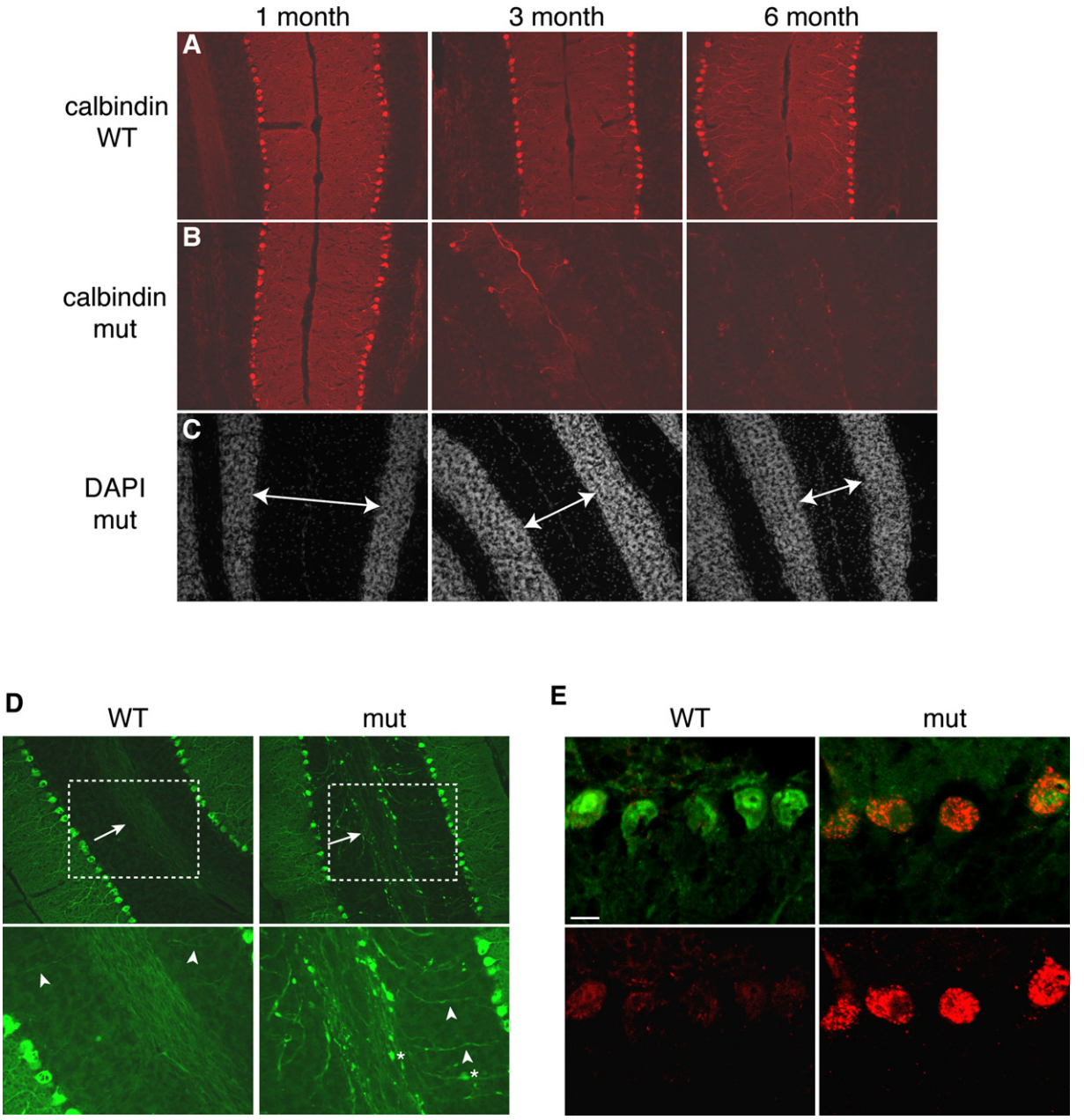

Figure 4. Degeneration of PCs in L7-Cre/*Mfn2*^{loxP} Cerebella

(A and B) Anti-calbindin IF. WT sections (A) show uniform layers of Purkinje cells at all ages. Mutant sections (B) are normal at 1 month, but show extensive degeneration by 3 months.

(C) DAPI staining of mutant sections from (B). DAPI stains cell nuclei and reveals a normal architecture of granule cells but a gradual reduction of the molecular layer (spanned by double-headed arrow).

(D) Anti-calbindin IF of 7-week-old cerebella. Arrows point to axon bundles running parallel to lines of Purkinje cell bodies. A magnified view (400×) of each boxed area shows individual axons (arrowheads) emanating from PCs. Mutant axons stain more brightly and have many focal swellings (asterisks), similar to those found in degenerating neurons of other systems.

(E) Anti-Complex V (red) and anti-calbindin (green) IF of 1-month-old cerebella. Mutants express much more Complex V than WT PCs. Scale bar represents 10 μm.

200× magnification in (A)–(D).

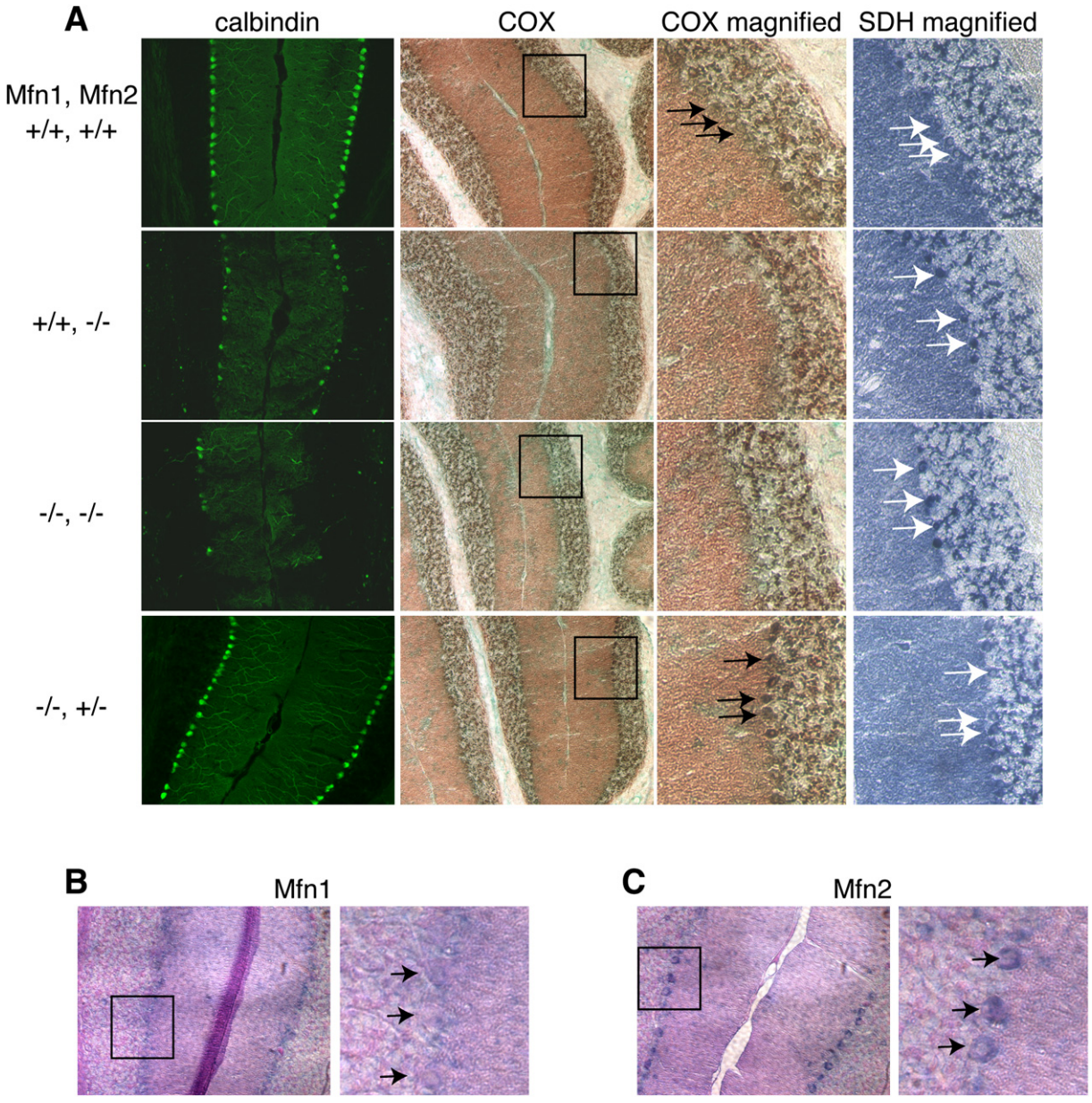

Figure 5. Electron Transport Chain Dysfunction and Mfn Expression in PCs

(A) 9-week-old L7-Cre/*Mfn*^{loxP} cerebella of the indicated genotypes analyzed by staining for calbindin, COX activity, and SDH activity. Anti-calbindin IF (green) shows that PCs lacking Mfn1 (bottom row) have normal architecture, indistinguishable from WT (top row). Mfn2 mutant animals (second row) have loss of PCs that is exacerbated by removal of Mfn1 (third row). COX$^+$ PCs (black arrows) are seen as dark brown circles forming a distinct monolayer between the brick-colored molecular layer and the speckled, darker granule cell layer. The COX panels are counterstained in green, and therefore COX$^-$ PCs (*Mfn2*$^{-/-}$) appear as a faint green stripe between the molecular and granule layers. SDH$^+$ PCs (white arrows) stain blue, with more staining per cell seen in *Mfn2*$^{-/-}$ cells. (Note however that there are fewer PCs in *Mfn2*$^{-/-}$ sections.) COX and SDH stains were performed on adjacent sections to show presence of PCs in absence of COX stain. A digitally magnified view of each boxed area is provided to more clearly show the Purkinje layer. (B and C) *Mfn* RNA in situ analysis of WT, adult cerebellum. Sections are counterstained with eosin (pink), and positive cells display purple staining. A digitally magnified view of each boxed area is provided. Arrows indicate the large, round cell bodies of PCs. Note that Purkinje cell bodies are clearly purple in the *Mfn2* in situ (C), but mostly pink in the *Mfn1* in situ (B). The majority of the *Mfn1* signal is non-Purkinje.
200× original magnification.

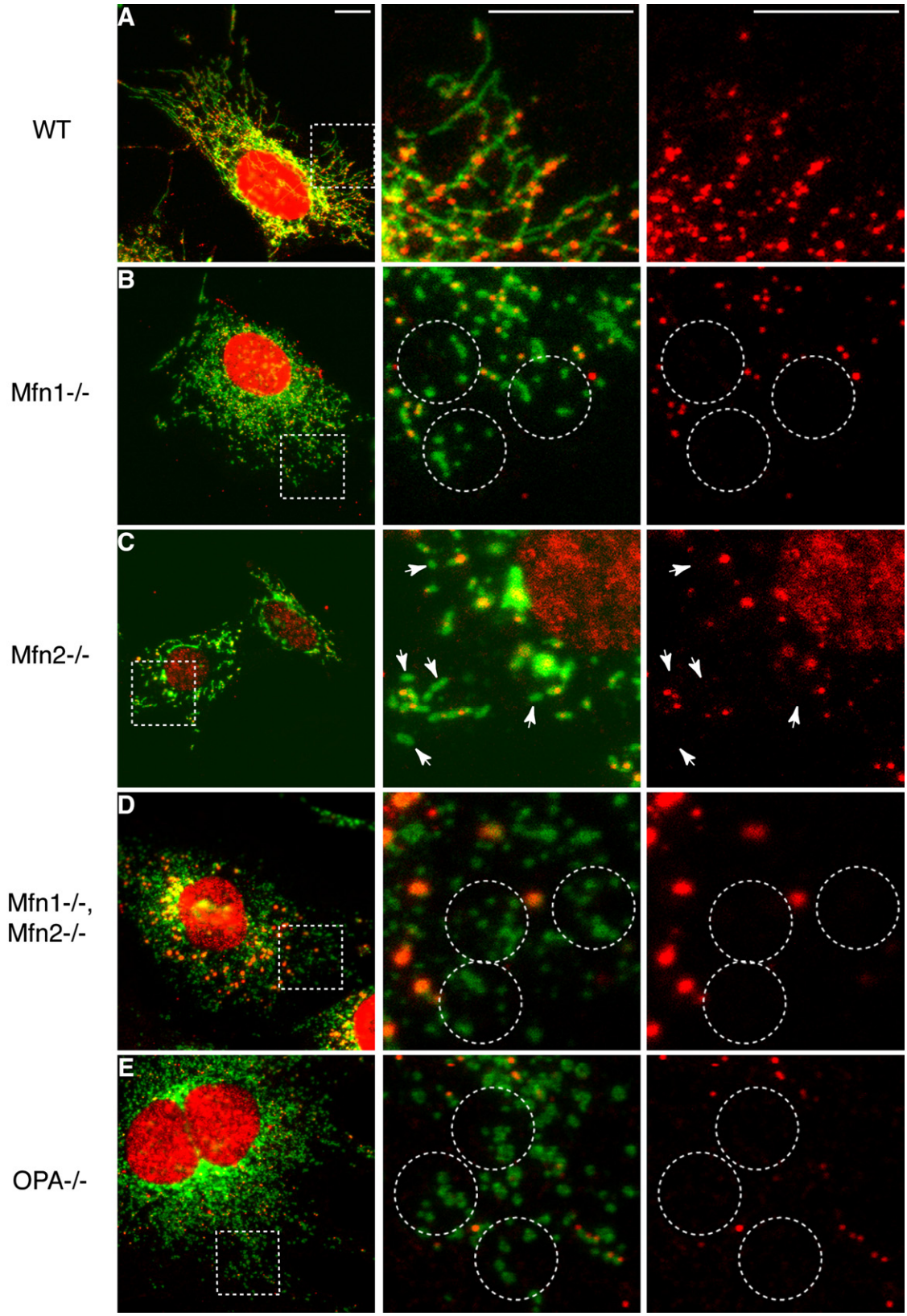
A
WT
B
Mfn1-/-
C
Mfn2-/-
D
Mfn1-/-,
Mfn2-/-
E
OPA-/-

DISCUSSION

Our observation that cerebellar Purkinje cells require Mfn2 directly supports emerging evidence that neurons are particularly sensitive to perturbations in mitochondrial dynamics (Chan, 2006; Chen and Chan, 2006). For example, CMT2A and DOA are two human neurodegenerative diseases caused by mutations in mitochondrial fusion genes. What cellular mechanisms underlie this connection between mitochondrial fusion and neuronal survival? Our studies indicate that loss of mitochondrial fusion results in two main consequences that impact cellular survival - mitochondrial dysfunction and alterations in mitochondrial localization.

Cellular Consequences of Defective Mitochondrial Fusion

Previous studies of Mfn null fibroblasts suggested that continual mitochondrial content mixing, driven by fusion, plays a protective role for mitochondrial function (Chen et al., 2005). Mitochondrial dynamics enables individual mitochondria that have suffered stochastic loss of essential components to rapidly replenish their stores. This behavior ensures that cells maintain a relatively homogeneous population of functional mitochondria. However, if fusion is inhibited, stochastic losses become long-lived or even permanent, resulting in a mitochondrial population that is heterogeneous in function.

Here we have generalized and extended these findings. Neuronal in vivo studies show that Mfn2-deficient Purkinje cells have impaired respiratory complex activity and defects in inner membrane structure characteristic of respiratory dysfunction. Moreover, we have identified loss of mtDNA nucleoids in fusion-deficient cells as the likely basis of reduced respiratory function. In WT cells, lack of mtDNA is only sporadically found in a few small mitochondria (Legros et al., 2004). We propose that such nucleoid-deficient mitochondria are rare in normal cells because continual fusion redistributes mtDNA within the mitochondrial reticulum. In fusion-deficient cells, mitochondrial fragmentation results in a majority of mitochondria lacking mtDNA. These nucleoid-deficient mitochondria lack essential respiratory subunits encoded by mtDNA, and have no pathway for regaining either the requisite proteins or mtDNA. They consequently accumulate as a large population lacking electron transport activity. Fusion-deficient cells contain mtDNA, but the mtDNA is sequestered into a much smaller mitochondrial mass that is insufficient to support the respiratory requirements of the cell. These results clarify how mammalian cells possessing mtDNA can nevertheless lose respiratory function in the absence of mitochondrial fusion. This is in direct contrast to yeast, where loss of fusion results in wholesale loss of mtDNA (Hermann et al., 1998).

Mitochondrial fusion is also required for proper mitochondrial distribution in neurons. Mfn null fibroblasts show a dramatic defect in directed movement of mitochondria (Chen et al., 2003). In mutant neurons, where the cell morphology includes extremely long, branched processes, this reduced motility likely underlies the paucity of mitochondria in neurites. Interestingly, in in vitro sensory neuron cultures, mitochondria with low membrane potential are preferentially transported toward the cell body (Miller and Sheetz, 2004). Because lack of mitochondrial fusion causes loss of membrane potential (Chen et al., 2005), such selective transport may also shift the distribution of mitochondria away from synaptic termini in fusion-deficient neurons.

Critical Dependence of Certain Neurons on Mitochondrial Fusion

Given that mitochondrial fusion is thought to be a universal process, why are particular neurons selectively affected by defects in mitochondrial fusion? We believe certain neurons have unique characteristics that cannot tolerate the underlying defects of reduced mitochondrial function and aberrant mitochondrial distribution. For example, PC dendrites branch more extensively than those of any other neuron in the brain. Our EM studies suggest that occlusion by clumped mitochondria can occur at these junctions, and might prevent further migration of essential cargoes/organelles down the tracts. In Alzheimer's disease, similar blockage of neuritic branch points by β-amyloid deposits has been suggested as a mechanism for neurodegeneration (Stokin et al., 2005). The motor neurons affected in CMT2A also have extreme cell geometry. Only those motor and sensory neurons with the longest axons - several feet in length - are affected. Over such long distances, attenuation of motility could easily translate into a dearth of mitochondria at axonal ends. Indeed, a recent study reported abnormal mitochondrial trafficking in sensory neurons with CMT2A mutant Mfn2 (Baloh et al., 2007).

Cell-type sensitivity to mutations in *Mfn2*, as seen in CMT2A and our knockout mice, probably also reflects the differential tissue expression of *Mfn1* and *Mfn2*. It is the total Mfn complement that controls the level of mitochondrial fusion (Detmer and Chan, 2007), but when expression of *Mfn1* and *Mfn2* are unequal, cells are more vulnerable to a mutation in one of the genes. Supporting this paradigm, *Mfn2* is expressed at significantly greater levels in PCs than is *Mfn1*, and therefore mutations in *Mfn2* cause mitochondrial dysfunction and neurodegeneration, whereas Mfn1 null PCs are viable and contain normal mitochondria. However, overexpression of Mfn1 in Mfn2 null PCs rescues PC viability, because it increases the total Mfn complement, and thus fusion activity.

Figure 6. Heterogeneous Loss of mtDNA Nucleoids in Fusion-Deficient Mitochondria

MEFs of the indicated genotypes were examined for co-localization of mitochondria (EGFP-OMP25, green) and mtDNA nucleoids (anti-DNA, red). Boxed areas are magnified as merged and red channel images. Circles and arrows highlight examples of mitochondria devoid of mtDNA nucleoids. Scale bars represent 10 μm.

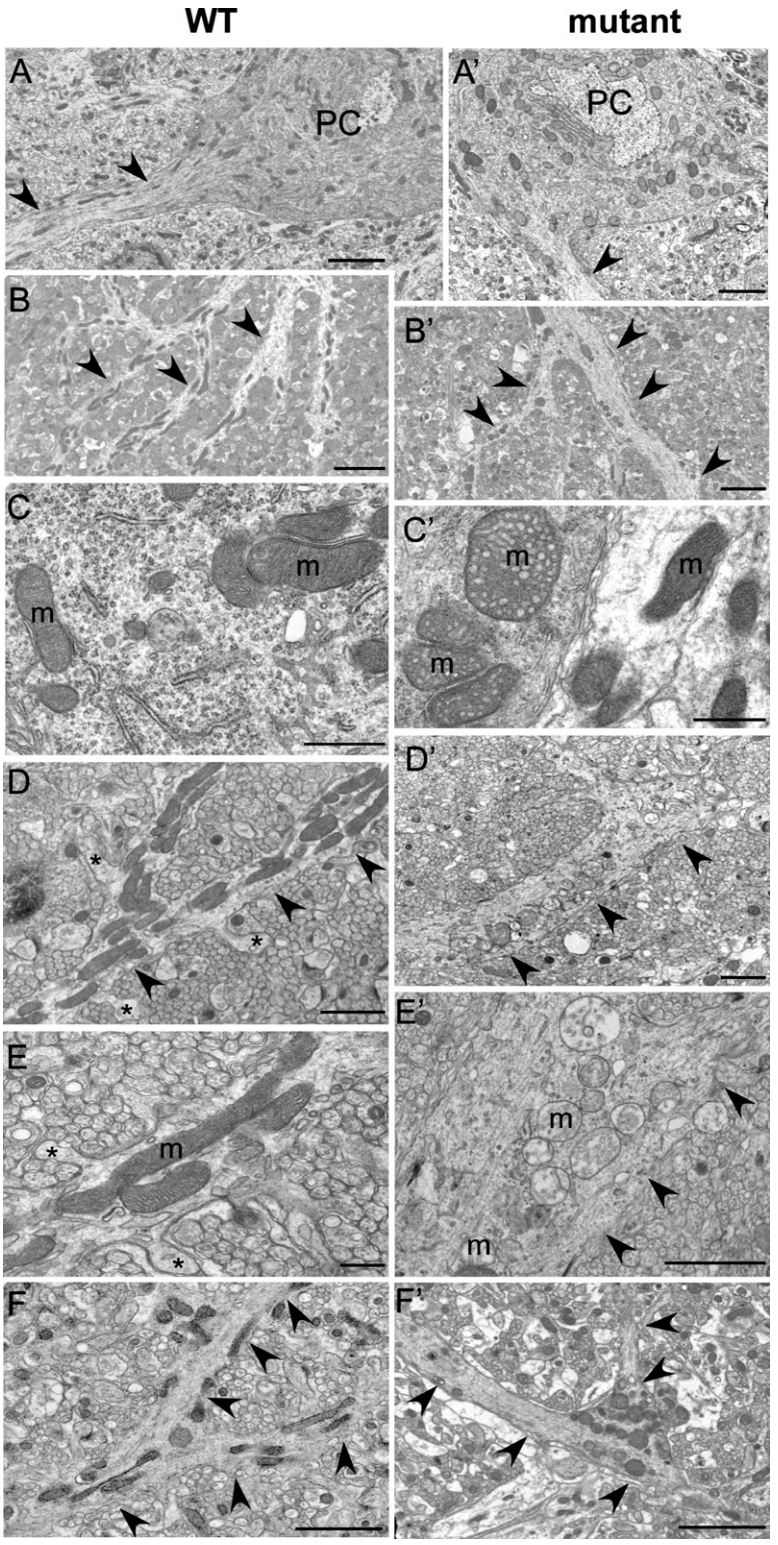

Figure 7. Ultrastructural Defects in En1-Cre/*Mfn2*^{loxP} and L7-Cre/*Mfn2*^{loxP} Cerebella

(A and B) EM images showing mitochondrial distribution in the cell body (A) and dendritic tracts (B) of 7-week-old WT and L7-Cre/*Mfn2*^{loxP} mutant PCs. Mutant mitochondria are notably clustered and less prevalent in the dendritic tracks (arrowheads).

(C) Organized cristae in WT mitochondria and vesiculated inner membranes in L7-Cre/*Mfn2*^{loxP} mutant mitochondria. In the mutant, note the juxtaposition of a tract with abnormal mitochondria to one with relatively normal mitochondria, highlighting the variability seen among PCs at this early age.

(D and E) Dendritic tracks of P10 WT and En1-Cre/*Mfn2*^{loxP} mutant PCs. Mutant dendritic tracks show clustering of swollen mitochondria lacking organized cristae. WT dendritic processes have abundant spines (asterisks), which are sparse in mutant samples.

(F) Mitochondria at dendritic junctions in L7-Cre/*Mfn2*^{loxP} PCs. WT mitochondria are found throughout smaller branches. Mutant mitochondria congregate at the triangular branch point and are rarely found further downstream.

Abbreviations are as follows: PC, Purkinje cell body; m, mitochondria; arrowheads, dendritic track; asterisk, dendritic spine.

Scale bars represent, respectively, (A)–(B′) = 5.0 μm; (C) and (C′) = 1.0 μm; (D), (D′), and (E′) = 0.2 μm; (E), (F), and (F′) = 0.5 μm.

Our studies on the mouse cerebellum provide insight into the cellular mechanisms through which perturbations in mitochondrial fusion lead to neurodegeneration. The in vivo and in vitro systems described here provide a readily manipulable experimental system to further dissect this relationship. Future work should be directed at examining to what extent these mechanisms contribute to the neurodegeneration found in CMT2A and DOA.

EXPERIMENTAL PROCEDURES

Mouse Experiments

To generate the *Mfn*^{loxP} conditional mice, ES clones (129 strain) carrying targeted mutations were injected into C57BL/6 blastocysts by Ingenious Laboratory. Founder chimeric mice were bred to Black Swiss mice, and agouti offspring were bred to FLPeR mice (Farley et al., 2000) to remove the neomycin resistance cassette. Resulting mice were maintained as homozygous stocks. Mouse strains have been deposited at the Mutant Mouse Regional Resource Centers (MMRRC). In all experiments, the Cre line was mated to the original knockout line (*Mfn*^{null}) to generate double heterozygotes. These mice were then mated to the relevant Mfn conditional line (*Mfn*^{loxP}) to generate experimental litters. This breeding scheme ensures more effective recombination of *loxP* sites. All controls were phenotypic WT littermates of the mutant animals. All experiments were approved by the Caltech Institutional Animal Care and Use Committee.

For rotarod analysis, mice were trained by running 3 trials/day, at a constant 24 rpm, for 3 consecutive days. They were tested on the fourth day and every 7 days thereafter. During the experimental runs, an acceleration test from 20–36 rpm was used.

Histological Analysis

For all but the histochemical stains, mice were perfused with fixative, and the brains were dissected, cut midsagittally, and embedded. TUNEL (ApopTag,Chemicon International) analysis was performed on formalin/paraffin sections. RNA in situ analysis was performed as described previously (Vortkamp et al., 1996). *Mfn* riboprobes were derived from the first heptad repeat region of each gene. No specific staining was detected using sense probes. For IF, formalin-fixed brains were cryosectioned, incubated with antibody and stained with DAPI. COX/SDH/NADH staining was performed on fresh frozen tissues, following protocols from the Washington University Neuromuscular Disease Center web site (http://www.neuro.wustl.edu/neuromuscular/index.html). After COX staining, sections were counterstained with Light Green (Biomeda).

For area measurements, hematoxylin and eosin stained sections were imaged and hand-traced using Adobe Illustrator. Area was calculated in arbitrary units using Image J software from the NIH.

Antibodies

Primary antibodies used include the following: mouse anti-calbindin (Sigma), rabbit anti-calbindin (Chemicon), anti-TAG1 (M. Yamamoto, DSHB/NICHD), anti-Complex V $F_1\alpha$-subunit (Molecular Probes), and anti-DNA (Chemicon). Secondary antibodies used include: Cy3-sheep anti-mouse (Jackson) and Alexa Fluor 488-goat anti-rabbit (Molecular Probes).

Cerebellar Cultures

Mixed cultures were established by a modified version of the protocol described previously (Hatten, 1985). In brief, cerebella were dissected from P1 pups and individually digested with trypsin and DNase. Trituration in DNase was followed by a soft spin. Cells were resuspended in dilute DNase and spun again. The final cell pellet was resuspended and plated into chambered slides (Lab-Tek). In experiments involving lentiviral expression, viral supernatants were added to the media at this time. Lentiviral constructs for Mfn1, Mfn2 and mito-DsRed were cloned into the lentiviral expression vector FUH_2B (gift of Carlos Lois, MIT). Retroviral stocks were produced as described (Lois et al., 2002), except that viral supernatants were collected in cerebellar culture media. Genotypes were determined by PCR analysis of tail DNA.

Imaging

For conventional microscopy, images were acquired using a Spot RT camera (Diagnostic Instruments, Inc.). For confocal imaging, images were acquired with a plan NeoFluar 63X NA 1.25 oil immersion objective on a laser-scanning 410 confocal microscope (Carl Zeiss MicroImaging, Inc.). LSM software was used for image acquisition, and Photoshop CS (Adobe) was used for pseudocoloring.

For EM, mice were perfused with 3% paraformaldehyde, 1.5% glutaraldehyde, 100 mM cacodylate, 2.5% sucrose, (pH 7.4), and post-fixed for 1 hr. Cerebellar sections were processed as described (McCaffery and Farquhar, 1995). They were post fixed in Palade's OsO4, *en bloc* stained in Kellenberger's uranyl acetate, dehydrated, and flat-embedded in epon. 80 nm en face sections were prepared on a Leica UCT ultramicrotome, collected onto 400 mesh high transmission nickel grids, and post stained with lead and uranyl acetate. Images were collected on a Philips EM 410 TEM equipped with a Soft Imaging System Megaview III digital camera.

Morphometry and Quantification

Morphometric analysis of dendritic tracks and spines was carried out utilizing analySIS v. 3.2 from Soft Imaging System (Lakewood, CO). The linear membrane length of 25 dendritic tracks was measured, and the dendritic spines were totaled. To eliminate questionable protrusions deriving from random undulations in the cell membrane and tangential planes of section, a lateral protrusion was determined to be a spine only if it exceeded 0.5 μm in length.

Supplemental Data

Supplemental Data include four figures, two tables, and three movies and can be found with this article online at http://www.cell.com/cgi/content/full/130/3/548/DC1/.

ACKNOWLEDGMENTS

We are grateful to Dr. M. E. Hatten for invaluable discussions about cerebellar development and Dr. T. Tomoda for helpful advice in experimental techniques. We thank Drs. S. Dymecki, H. Westphal, P. Soriano, A. McMahon, A. Joyner, and W. Wisden for their generous sharing of mouse strains. We thank S. Detmer for reviewing the manuscript. We appreciate D. Solis for her care of and keen observation of our animals. This work was supported by NIH grant GM062967 and the United Mitochondrial Disease Foundation.

Received: February 16, 2007
Revised: May 11, 2007
Accepted: June 12, 2007
Published: August 9, 2007

REFERENCES

Alavi, M.V., Bette, S., Schimpf, S., Schuettauf, F., Schraermeyer, U., Wehrl, H.F., Ruttiger, L., Beck, S.C., Tonagel, F., Pichler, B.J., et al. (2007). A splice site mutation in the murine Opa1 gene features pathology of autosomal dominant optic atrophy. Brain *130*, 1029–1042.

Alexander, C., Votruba, M., Pesch, U.E., Thiselton, D.L., Mayer, S., Moore, A., Rodriguez, M., Kellner, U., Leo-Kottler, B., Auburger, G., et al. (2000). OPA1, encoding a dynamin-related GTPase, is mutated in autosomal dominant optic atrophy linked to chromosome 3q28. Nat. Genet. *26*, 211–215.

Aller, M.I., Jones, A., Merlo, D., Paterlini, M., Meyer, A.H., Amtmann, U., Brickley, S., Jolin, H.E., McKenzie, A.N., Monyer, H., et al. (2003). Cerebellar granule cell Cre recombinase expression. Genesis *36*, 97–103.

Arnoult, D., Grodet, A., Lee, Y.J., Estaquier, J., and Blackstone, C. (2005). Release of OPA1 during apoptosis participates in the rapid and complete release of cytochrome c and subsequent mitochondrial fragmentation. J. Biol. Chem. *280*, 35742–35750.

Baloh, R.H., Schmidt, R.E., Pestronk, A., and Milbrandt, J. (2007). Altered axonal mitochondrial transport in the pathogenesis of Charcot-Marie-Tooth disease from mitofusin 2 mutations. J. Neurosci. *27*, 422–430.

Barski, J.J., Dethleffsen, K., and Meyer, M. (2000). Cre recombinase expression in cerebellar Purkinje cells. Genesis *28*, 93–98.

Baurle, J., and Grusser-Cornehls, U. (1994). Axonal torpedoes in cerebellar Purkinje cells of two normal mouse strains during aging. Acta Neuropathol. (Berl.) *88*, 237–245.

Bereiter-Hahn, J., and Voth, M. (1994). Dynamics of mitochondria in living cells: shape changes, dislocations, fusion, and fission of mitochondria. Microsc. Res. Tech. *27*, 198–219.

Chan, D.C. (2006). Mitochondria: dynamic organelles in disease, aging, and development. Cell *125*, 1241–1252.

Chen, H., and Chan, D.C. (2006). Critical dependence of neurons on mitochondrial dynamics. Curr. Opin. Cell Biol. *18*, 453–459.

Chen, H., Chomyn, A., and Chan, D.C. (2005). Disruption of fusion results in mitochondrial heterogeneity and dysfunction. J. Biol. Chem. *280*, 26185–26192.

Chen, H., Detmer, S.A., Ewald, A.J., Griffin, E.E., Fraser, S.E., and Chan, D.C. (2003). Mitofusins Mfn1 and Mfn2 coordinately regulate mitochondrial fusion and are essential for embryonic development. J. Cell Biol. *160*, 189–200.

Chizhikov, V., and Millen, K.J. (2003). Development and malformations of the cerebellum in mice. Mol. Genet. Metab. *80*, 54–65.

Cipolat, S., Martins de Brito, O., Dal Zilio, B., and Scorrano, L. (2004). OPA1 requires mitofusin 1 to promote mitochondrial fusion. Proc. Natl. Acad. Sci. USA *101*, 15927–15932.

Danielian, P.S., Muccino, D., Rowitch, D.H., Michael, S.K., and McMahon, A.P. (1998). Modification of gene activity in mouse embryos in utero by a tamoxifen-inducible form of Cre recombinase. Curr. Biol. *8*, 1323–1326.

Davies, V.J., Hollins, A.J., Piechota, M.J., Yip, W., Davies, J.R., White, K.E., Nicols, P.P., Boulton, M.E., and Votruba, M. (2007). Opa1 deficiency in a mouse model of Autosomal Dominant Optic Atrophy impairs mitochondrial morphology, optic nerve structure and visual function. Hum. Mol. Genet. *16*, 1307–1318.

Delettre, C., Lenaers, G., Griffoin, J.M., Gigarel, N., Lorenzo, C., Belenguer, P., Pelloquin, L., Grosgeorge, J., Turc-Carel, C., Perret, E., et al. (2000). Nuclear gene OPA1, encoding a mitochondrial dynamin-related protein, is mutated in dominant optic atrophy. Nat. Genet. *26*, 207–210.

Detmer, S.A., and Chan, D.C. (2007). Complementation between mouse Mfn1 and Mfn2 protects mitochondrial fusion defects caused by CMT2A disease mutations. J. Cell Biol. *176*, 405–414.

Farley, F.W., Soriano, P., Steffen, L.S., and Dymecki, S.M. (2000). Widespread recombinase expression using FLPeR (flipper) mice. Genesis *28*, 106–110.

Frezza, C., Cipolat, S., Martins de Brito, O., Micaroni, M., Beznoussenko, G.V., Rudka, T., Bartoli, D., Polishuck, R.S., Danial, N.N., De Strooper, B., et al. (2006). OPA1 controls apoptotic cristae remodeling independently from mitochondrial fusion. Cell *126*, 177–189.

Guo, X., Macleod, G.T., Wellington, A., Hu, F., Panchumarthi, S., Schoenfield, M., Marin, L., Charlton, M.P., Atwood, H.L., and Zinsmaier, K.E. (2005). The GTPase dMiro is required for axonal transport of mitochondria to Drosophila synapses. Neuron *47*, 379–393.

Hatten, M.E. (1985). Neuronal regulation of astroglial morphology and proliferation in vitro. J. Cell Biol. *100*, 384–396.

Hermann, G.J., Thatcher, J.W., Mills, J.P., Hales, K.G., Fuller, M.T., Nunnari, J., and Shaw, J.M. (1998). Mitochondrial fusion in yeast requires the transmembrane GTPase Fzo1p. J. Cell Biol. *143*, 359–373.

Kimmel, R.A., Turnbull, D.H., Blanquet, V., Wurst, W., Loomis, C.A., and Joyner, A.L. (2000). Two lineage boundaries coordinate vertebrate apical ectodermal ridge formation. Genes Dev. *14*, 1377–1389.

Laine, J., and Axelrad, H. (1994). The candelabrum cell: a new interneuron in the cerebellar cortex. J. Comp. Neurol. *339*, 159–173.

Lakso, M., Pichel, J.G., Gorman, J.R., Sauer, B., Okamoto, Y., Lee, E., Alt, F.W., and Westphal, H. (1996). Efficient in vivo manipulation of mouse genomic sequences at the zygote stage. Proc. Natl. Acad. Sci. USA *93*, 5860–5865.

Legros, F., Malka, F., Frachon, P., Lombes, A., and Rojo, M. (2004). Organization and dynamics of human mitochondrial DNA. J. Cell Sci. *117*, 2653–2662.

Li, Z., Okamoto, K., Hayashi, Y., and Sheng, M. (2004). The importance of dendritic mitochondria in the morphogenesis and plasticity of spines and synapses. Cell *119*, 873–887.

Lois, C., Hong, E.J., Pease, S., Brown, E.J., and Baltimore, D. (2002). Germline transmission and tissue-specific expression of transgenes delivered by lentiviral vectors. Science *295*, 868–872.

McCaffery, J.M., and Farquhar, M.G. (1995). Localization of GTPases by indirect immunofluorescence and immunoelectron microscopy. Methods Enzymol. *257*, 259–279.

Miller, K.E., and Sheetz, M.P. (2004). Axonal mitochondrial transport and potential are correlated. J. Cell Sci. *117*, 2791–2804.

Niemann, A., Ruegg, M., La Padula, V., Schenone, A., and Suter, U. (2005). Ganglioside-induced differentiation associated protein 1 is a regulator of the mitochondrial network: new implications for Charcot-Marie-Tooth disease. J. Cell Biol. *170*, 1067–1078.

Olichon, A., Baricault, L., Gas, N., Guillou, E., Valette, A., Belenguer, P., and Lenaers, G. (2003). Loss of OPA1 perturbates the mitochondrial inner membrane structure and integrity, leading to cytochrome c release and apoptosis. J. Biol. Chem. *278*, 7743–7746.

Sotelo, C. (2004). Cellular and genetic regulation of the development of the cerebellar system. Prog. Neurobiol. *72*, 295–339.

Stokin, G.B., Lillo, C., Falzone, T.L., Brusch, R.G., Rockenstein, E., Mount, S.L., Raman, R., Davies, P., Masliah, E., Williams, D.S., et al. (2005). Axonopathy and transport deficits early in the pathogenesis of Alzheimer's disease. Science *307*, 1282–1288.

Stowers, R.S., Megeath, L.J., Gorska-Andrzejak, J., Meinertzhagen, I.A., and Schwarz, T.L. (2002). Axonal transport of mitochondria to synapses depends on milton, a novel Drosophila protein. Neuron *36*, 1063–1077.

Sugioka, R., Shimizu, S., and Tsujimoto, Y. (2004). Fzo1, a protein involved in mitochondrial fusion, inhibits apoptosis. J. Biol. Chem. *279*, 52726–52734.

Tallquist, M.D., and Soriano, P. (2000). Epiblast-restricted Cre expression in MORE mice: a tool to distinguish embryonic vs. extra-embryonic gene function. Genesis *26*, 113–115.

Verhoeven, K., Claeys, K.G., Zuchner, S., Schroder, J.M., Weis, J., Ceuterick, C., Jordanova, A., Nelis, E., De Vriendt, E., Van Hul, M., et al. (2006). MFN2 mutation distribution and genotype/phenotype correlation in Charcot-Marie-Tooth type 2. Brain *129*, 2093–2102.

Verstreken, P., Ly, C.V., Venken, K.J., Koh, T.W., Zhou, Y., and Bellen, H.J. (2005). Synaptic mitochondria are critical for mobilization of reserve pool vesicles at Drosophila neuromuscular junctions. Neuron *47*, 365–378.

Vortkamp, A., Lee, K., Lanske, B., Segre, G.V., Kronenberg, H.M., and Tabin, C.J. (1996). Regulation of rate of cartilage differentiation by Indian hedgehog and PTH-related protein. Science *273*, 613–622.

Wallace, D.C. (1999). Mitochondrial diseases in man and mouse. Science *283*, 1482–1488.

Zuchner, S., Mersiyanova, I.V., Muglia, M., Bissar-Tadmouri, N., Rochelle, J., Dadali, E.L., Zappia, M., Nelis, E., Patitucci, A., Senderek, J., et al. (2004). Mutations in the mitochondrial GTPase mitofusin 2 cause Charcot-Marie-Tooth neuropathy type 2A. Nat. Genet. *36*, 449–451.